Hindawi Publishing Corporation
Advances in High Energy Physics
Volume 2012, Article ID 350150, 12 pages
doi:10.1155/2012/350150

Research Article

The Results of Search for the Neutrino Magnetic Moment in GEMMA Experiment

A. G. Beda,[1] V. B. Brudanin,[2] V. G. Egorov,[2] D. V. Medvedev,[2] V. S. Pogosov,[2,3] M. V. Shirchenko,[2] and A. S. Starostin[1]

[1] *State Science Center, Institute for Theoretical and Experimental Physics (ITEP), 117218 Moscow, Russia*
[2] *Laboratory of Nuclear Problems (LNP), Joint Institute for Nuclear Research (JINR), 141980 Dubna, Russia*
[3] *Alikhanyan National Laboratory (ANL), Yerevan Physics Institute (YerPhI), 375036 Yerevan, Armenia*

Correspondence should be addressed to D. V. Medvedev, chess1984@mail.ru

Received 27 December 2011; Revised 16 March 2012; Accepted 2 April 2012

Academic Editor: Arthur B. McDonald

The result of the neutrino magnetic moment measurement at the Kalinin Nuclear Power Plant (KNPP) with GEMMA spectrometer is presented. The antineutrino-electron scattering is investigated. A high-purity germanium detector with a mass of 1.5 kg placed at a distance of 13.9 m from the 3 GW_{th} reactor core is exposed to the antineutrino flux of 2.7×10^{13} $1/cm^2/s$. The recoil electron spectra taken in 18134 and 4487 hours for the reactor ON and OFF periods are compared. The upper limit for the neutrino magnetic moment $\mu_\nu < 2.9 \times 10^{-11}\,\mu_B$ at 90% C.L. is derived from the data processing.

1. Introduction

The Minimally Extended Standard Model (MSM) predicts a very small magnetic moment value for the massive neutrino ($\mu_\nu \sim 10^{-19}\,\mu_B$) that cannot be observed in experiment at present. However, there are a number of theory extensions beyond the MSM where NMM could be at the level of $10^{-(10\div12)}\,\mu_B$ [1–5] for Majorana neutrino. At the same time, it follows from general considerations [6, 7] that the Dirac NMM cannot exceed $10^{-14}\,\mu_B$. Therefore, the observation of NMM value higher than $10^{-14}\,\mu_B$ would be an evidence of new physics and indicate undoubtedly [8–10] that neutrino is a Majorana particle. Furthermore, according to [11] new lepton number violating physics responsible for the generation of NMM arises at the scale Λ which is well below the see-saw scale. For example, for $\mu_\nu = 1.0 \times 10^{-11}\,\mu_B$ and the neutrino mass $m_\nu = 0.3$ eV, we can find that $\Lambda \leq 100$ TeV.

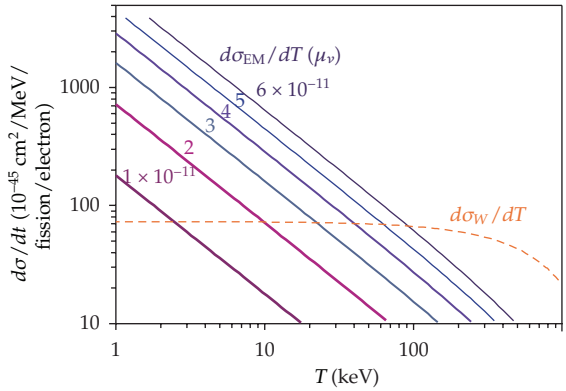

Figure 1: Weak (W) and electromagnetic (EM) cross-sections calculated for several NMM values.

It is rather important to make laboratory NMM measurements sensitive enough to reach the $\sim 10^{-11}\ \mu_B$ region. The Savanna River experiment by Reines' group can be considered as the beginning of such measurements. Over a period of thirty years, the sensitivity of reactor experiments has been improved by only a factor of three: from $[2-4] \times 10^{-10}\ \mu_B$ [12, 13] to $[6-7] \times 10^{-11}\ \mu_B$ [14, 15]. Similar limits were obtained for solar neutrinos [16, 17], but, due to the MSW effect (as well as matter-enhanced oscillations in the Sun), their flavor composition changes and therefore the solar NMM results could differ from the reactor ones. In this paper, the result of NMM measurement by the collaboration of ITEP (Moscow) and JINR (Dubna) is presented. The measurements are carried out with the GEMMA spectrometer [15, 18, 19] at the $3\,\mathrm{GW_{th}}$ reactor of the KNPP.

2. Experimental Approach

A laboratory measurement of the NMM is based on its contribution to the $\nu - e$ scattering. For nonzero NMM, the $\nu - e$ differential cross-section is [8] a sum of weak interaction cross-section ($d\sigma^W/dT$) and electromagnetic one ($d\sigma^{\mathrm{EM}}/dT$):

$$\frac{d\sigma^W}{dT} = G_F^2 \cdot \left(\frac{m}{2\pi}\right) \cdot \left[4x^4 + \left(1+2x^2\right)^2 \cdot \left(1-\frac{T}{E}\right)^2 - \frac{2x^2\left(1+x^2\right)mT}{E^2}\right], \tag{2.1}$$

$$\frac{d\sigma^{\mathrm{EM}}}{dT} = \pi r_0^2 \left(\frac{\mu_\nu}{\mu_B}\right)^2 \left(\frac{1}{T} - \frac{1}{E}\right), \tag{2.2}$$

where E is the incident neutrino energy, T is the electron recoil energy, $x^2 = \sin^2\theta_W = 0,232$ is a Weinberg parameter, and r_0 is a classical electron radius ($\pi r_0^2 = 2.495 \times 10^{-25}\ \mathrm{cm}^2$).

Figure 1 shows differential cross-sections (2.1) and (2.2) averaged over the typical antineutrino reactor spectrum versus the electron recoil energy. One can see that, at low recoil energy ($T \ll E_\nu$), the value of $d\sigma^W/dT$ becomes almost constant while $d\sigma^{\mathrm{EM}}/dT$ increases as T^{-1}. It becomes evident that the lower the detector threshold is, the more considerable increase in the NMM effect with respect to the weak unremovable contribution we can obtain.

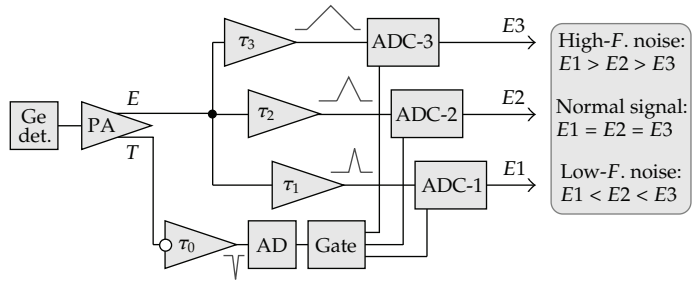

Figure 2: Signal processing scheme.

To realize this useful feature in our GEMMA spectrometer [15], we use a 1.5 kg HPGe detector with the energy threshold as low as 2.8 keV. To be sure that there is no efficiency cut at this energy, the "hard" trigger threshold is set twice lower (1.5 keV).

The background suppression is realized by means of various methods. The detector (Figure 3) is placed inside a cup-shaped NaI crystal with 14 cm thick walls and surrounded by 5 cm of electrolytic copper and 15 cm of lead. This active and passive shielding reduces the external γ-background in the ROI (the region of interest (ROI) in our analysis includes two fragments from 2.8 to 9.4 and from 11.2 to 55 keV, i.e., the low-energy part of the continuous spectrum without peaks which could depend on the reactor operation) to the level of ~2 counts/keV/kg/day. Being located just under the reactor number 2 of KNPP (at the distance of 13.9 m from the reactor core center), the detector is well shielded against the hadronic component of cosmic rays by the reactor body and technologic equipment (overburden ~70 m w.e.). The muon component is reduced by a factor of 10 at ±20° with respect to vertical line and 3 at 70°÷ 80°. Nevertheless, a part of residual muons is captured in the massive shielding and produce neutrons that scatter elastically in Ge detector and raise the low-energy background. To suppress this effect, the spectrometer is covered with additional plastic scintillator plates which produce relatively long μ-veto signals. In order to reduce nonphysical low-amplitude circuit noise (afterpulses, radio frequency interference, microphonism, etc.), the detector signal is processed by three parallel independent electronic channels with different shaping time (Figure 2). This allows us to apply a primitive Fourier analysis [20] and thus discriminate the artefact signals.

3. Data Taking and Processing

In order to get a recoil electron spectrum, we use a differential method comparing the spectra measured at the reactor operation (ON) and shut down (OFF) periods. Our experiment is divided into 3 phases. For Phase-I, we have 5184 and 1853 hours for the reactor ON and OFF periods, respectively. 6798 ON-hours and 1021 OFF-hours of live time statistics have been found to be available for analysis in Phase-II. Today, we can add Phase-III results. They contain 6152 ON-hours and 1613 OFF-hours of live time statistics.

During the measurement, the signals of the HPGe detector, anticompton NaI shielding, and outer anticosmic plastic counters as well as dead time information are collected on the event by event basis. The detection efficiency just above the threshold is checked with a pulser. The neutrino flux during the ON period is estimated via the reactor thermal power measured with accuracy of 0.7%.

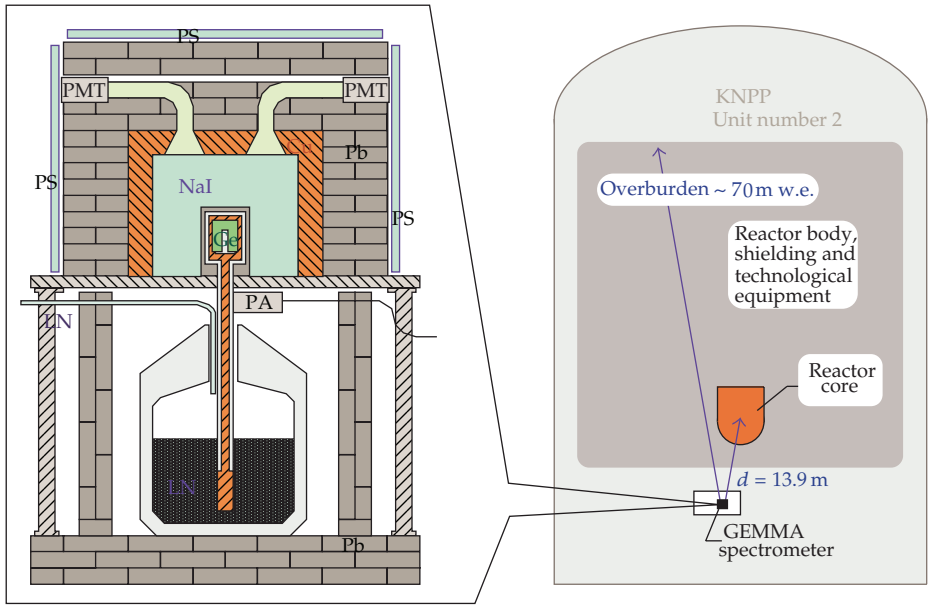

Figure 3: Ge detector inside the active (NaI, PS) and passive (Cu, Pb) shielding.

At the beginning of the experiment, the background was measured with and without shielding. On Figure 4, one can see the background suppression due to passive and active shielding.

The collected data are processed in several steps. The first step involves different selections aimed to suppress nonphysical and physical backgrounds.

(1) *Bad run* rejection. We reject those hour-long runs which correspond to the periods of liquid nitrogen filling and any mechanical or electrical work at the detector site as it could produce noise.

(2) *Radioactive noble gas* rejection. Unfortunately, the detector shielding turned out to be not tight enough against radioactive noble gases. To smooth away this design defect, we analyze energy spectra measured during each several hours and check the stability of the γ-background. If any visible excess of 81 keV (^{133}Xe), 250 keV (^{135}Xe) or 1294 keV (^{41}Ar) γ-line occurs, the corresponding runs are removed. (In fact these files are used later for the "noble gas" correction for the rest of the data.)

(3) *Detector noise* rejection. For some obscure reasons, our Ge detector happened to become noisy from time to time. In order to reject these noisy periods, the low-amplitude count rate is checked second by second and those seconds that contain more than 5 events with $E > 2$ keV are rejected.

(4) *Audio-frequency* rejection. We reject those events which are separated by a time interval shorter than 80 ms or equal to $[n \cdot (20.0 \pm 0.1)]$ ms. In this way, we suppress the noise caused by mechanical vibrations (ringing) and the 50 Hz power line frequency.

(5) *Fourier* rejection. As it has already been mentioned, the real and the artefact signals have different Fourier spectra. To exploit this difference, we build three plots similar to that shown in Figure 5: (E_2 versus E_1), (E_3 versus E_2), and (E_1 versus E_3).

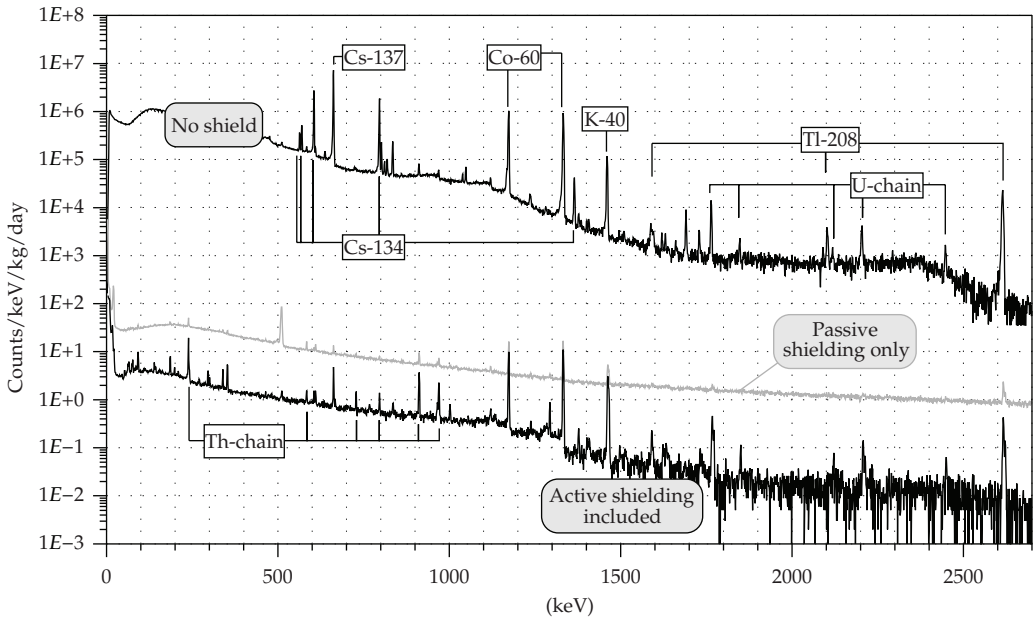

Figure 4: Gamma spectra measured at the detector site under different shielding conditions. ON and OFF reactor periods do not demonstrate any visible difference.

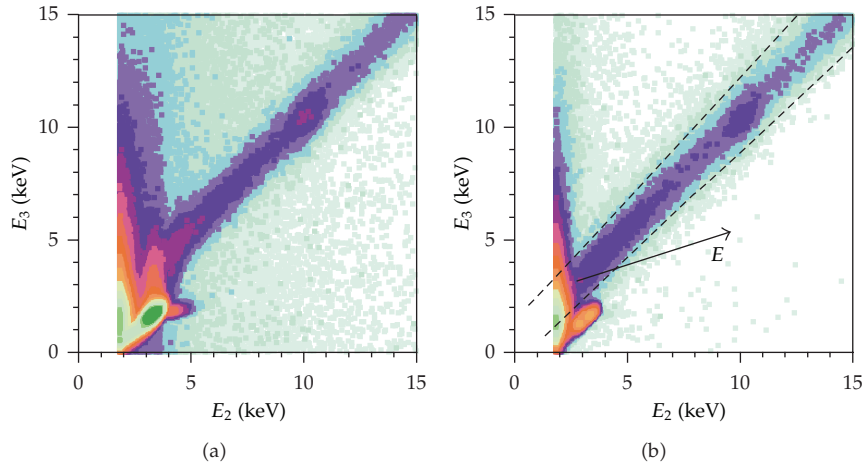

Figure 5: Example of the Fourier analysis made with different shaping times: ADC-2 operates with 4 μs pulses, and ADC-3 operates with 12 μs pulses. Plot (a) is made *before* and (b) *after* the "audio-frequency" rejection; one can see that most of the rejected events are nondiagonal. (The color intensity scale is logarithmic.)

The real signal falls into diagonals ($E_1 \simeq E_2 \simeq E_3$) within the energy resolution, whereas any nonphysical artefact shows a different pattern. We select only diagonal events and thus additionally reject low- and high-frequency noise. To ensure the best cutoff, we replace E_1, E_2, and E_3 by their linear combination E:

$$E = aE_1 + bE_2 + cE_3, \tag{3.1}$$

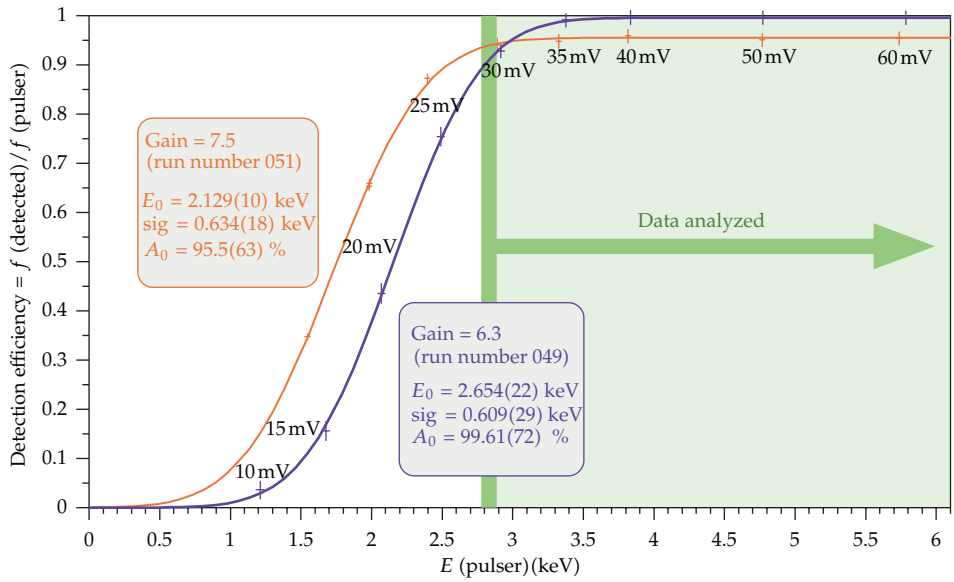

Figure 6: Low-energy threshold function measured with 50 Hz pulser at several amplitudes. Decreasing of the "hard" threshold minimizes the correction value but also decreases total detection efficiency (because of higher load and therefore higher dead time).

where the weights a, b, c are chosen (subjectively) so as to make the vector be antiparallel to the noise gradient (Figure 5(b)).

After the above rejections, we construct energy spectra for the ON and OFF periods and correct them in the following two steps (the corrections do not give a significant error to the final result as they affect ON and OFF spectra in the same way):

(1) *Noble gas* correction. As our spectrometer is not located in a special laboratory but in the technological room sometimes, there are short operational periods when the concentration of ^{41}Ar, ^{133}Xe, and ^{135}Xe in this room becomes higher than usual. Spectra measured under these conditions are used to evaluate the contribution of each radioactive gas to the low-energy part of the background. These contributions normalized to the intensities of the corresponding γ-lines are then subtracted from those few ON and OFF spectra where small traces of these lines are still present. In this case, the value of such correction in the ROI does not exceed 1-2%.

(2) *Low-energy* threshold correction. The detection efficiency η just above the threshold E_0 is measured with a pulser and is fitted with the function

$$\eta(E) = \int_{-\infty}^{E} \frac{1}{\sqrt{2\pi}\sigma} e^{-(x-E_0)^2/2\sigma^2} dx, \tag{3.2}$$

where σ stands for the detector energy resolution. Experimental spectra are then corrected by the function (3.2) which becomes significant at energies below 2.8 keV in our case (Figure 6).

During the long-term measurements, it is crucial to establish the long-term stability as well. In our case, this problem is divided into two main parts: the background constancy

and the hardware stability. The main source of background instability is the presence of noble gases (see "noble gas correction"). One of the best ways to check the hardware is to control the position of some energy peak because almost any changes in the hardware result in its shift. But, in the low background measurements, this method could not be applied due to insufficient statistics. That is why we have used the following procedure. First, we have made the binning of overall data. The idea of this binning consists in obtaining enough data in some devoted spectrum lines. The next step is to check if those peaks have some additional broadening because of possible amplification changes during the bin time. If this broadening appears to be large enough (10% or more), we perform the rebinning to find the exact time of the shift and possibly distinguish its origin. Then, the data divided in this way are transferred to the uniform energy scale (0.1 keV/channel) and only after that are summed up. Thus, we automatically reduce the influence of the hardware instability to the negligible level.

As a result, we obtain energy spectra S for the ON and OFF periods which must be normalized by the corresponding active times T_{ON} and T_{OFF} and then compare them to each other taking into account the additional neutrino dependent term:

$$\frac{S_{\mathrm{ON}}}{T_{\mathrm{ON}}} = \frac{S_{\mathrm{OFF}}}{T_{\mathrm{OFF}}} + m_d \Phi_\nu (W + X * \mathrm{EM}). \tag{3.3}$$

The last term includes the fiducial detector mass m_d and the antineutrino flux Φ_ν (known with an accuracy of 1.7% and 3.5%, resp.) multiplied by the sum of two neutrino contributions: the weak one (W) which can be calculated easily using formula (2.1) and is completely negligible in our case and the electromagnetic one (EM) which is proportional to the squared NMM value:

$$\mathrm{X} \equiv \left(\frac{\mu_\nu}{10^{-11} \mu_B} \right)^2. \tag{3.4}$$

Unfortunately, the exposition times of ON and OFF periods are not equal. A usual OFF period is much shorter, and therefore the final sensitivity is limited by the background uncertainties. However, today after four years of data taking, we know the ROI background structure with good confidence (280 kg*day of OFF statistics). It gives us the right to introduce additional information in our analysis, namely, to state that our background is *a smooth curve*.

To implement this conventional idea, we fit the background OFF spectrum in the ROI from 2.8 keV to 55 keV with a parametrized smooth function (e.g., a sum of Gaussian, exponential, and linear functions). We can also use splines for this procedure. All these fits produce slightly different results, and their spread is taken into account in the final systematic error.

Then, we compare the ON spectrum channel by channel with the obtained background curve and extract the X-value (or its upper limit) from (3.3). This evaluation is more complicated than expected because it is very difficult to count active times T_{ON} and T_{OFF} precisely in a proper way (especially after numerous selections of the events). To avoid possible errors caused by this procedure, we divide the active time normalization into two parts: absolute (T_{ON}) and relative ($\tau \equiv T_{\mathrm{ON}}/T_{\mathrm{OFF}}$).

Roughly, both the T_{ON} and T_{OFF} active times are estimated using several background γ-lines: the 238 keV line of ^{212}Pb, the 1173 keV and 1333 keV lines of ^{60}Co, and the 1461 keV line

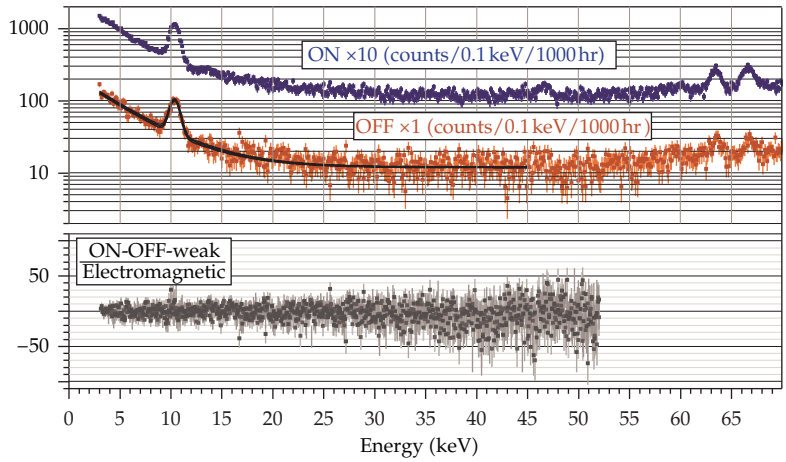

Figure 7: Fragments of the experimental ON and OFF spectra (top) and their difference normalized by the electromagnetic cross-section (bottom).

of ^{40}K. This radiation originates from the pollution of the internal parts of the spectrometer and is therefore stable in time and does not depend on the reactor operation. Comparing the intensities of the above lines measured *with* and *without* any selections, we get the estimates T'_{ON} and T'_{OFF} with an accuracy of 0.9% and 1.9%, respectively. However, this is not enough to evaluate the τ value with the required precision. We resolve this problem in the following way.

The relative ON/OFF time factor τ is represented as a product of its estimate $\tau' = T'_{\mathrm{ON}}/T'_{\mathrm{OFF}}$ (which is a constant known with an accuracy of 2.1%) and a correction factor K (which should be not far from 1.0): $\tau = K\tau'$. Then, (3.3) can be transformed to

$$W + X * \mathrm{EM} = \left(S_{\mathrm{ON}} - K\tau' S_{\mathrm{OFF}}\right) * \left(T_{\mathrm{ON}} m_d \Phi_\nu\right)^{-1}. \tag{3.5}$$

As one can see, the absolute time normalization T_{ON} contributes to the final result in the same way as Φ_ν or m_d (i.e., simply as a *factor*), and therefore we can replace T_{ON} by its estimate T'_{ON}. Standard systematic deviation δX caused by this factor is not significant:

$$\frac{\delta X}{X} = \frac{\delta\left(T_{\mathrm{ON}} m_d \Phi_\nu\right)}{T_{\mathrm{ON}} m_d \Phi_\nu} = \sqrt{(0.9\%)^2 + (1.7\%)^2 + (3.5\%)^2} \approx 4.0\%. \tag{3.6}$$

Preliminary time normalization can be performed not only with the background γ-lines but also with a part of the continuous spectrum (e.g., from 20 to 55 keV). Both methods give very similar results, but the second one provides better precision due to higher statistics. Comparison of γ-lines as well as integrals of continuous parts between ON and OFF spectra remaining after application of selection procedure allows us to extract K-value with accuracy better than 1%.

Figure 7 illustrates good background knowledge. Furthermore, its bottom part shows that there is no visible deviation of X-value from zero within statistical errors. This demonstrates that our way of data processing is adequate and does not bring in an additional systematic error.

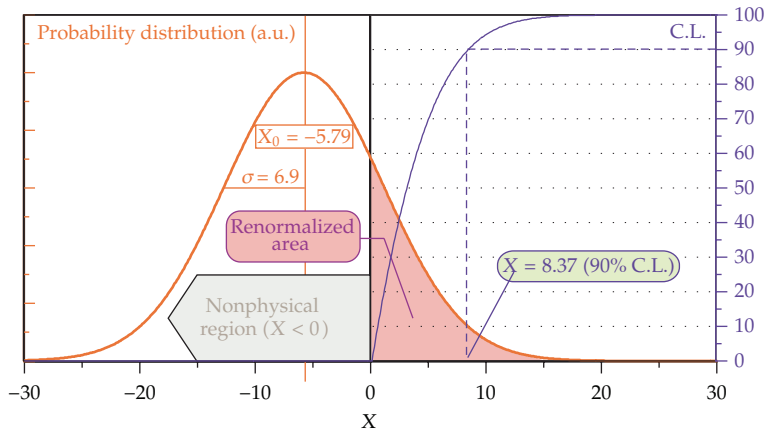

Figure 8: Final probability distribution of X.

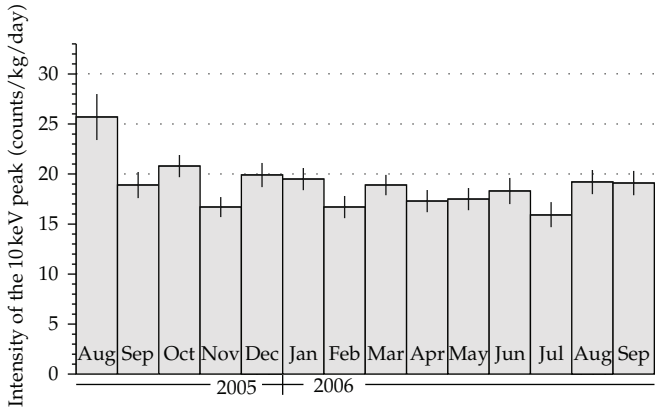

Figure 9: Variation of 10 keV peak intensity in time.

To extract the NMM value, we compare ON spectrum with the obtained curve channel by channel (to be more precise, with a narrow corridor with the width given by the fitting uncertainty). Applying this procedure to the total statistics of Phases I + II + III, we get the final distribution for X (Figure 8).

After a conventional renormalization recommended by the Particle Data Group [21] and described in our previous work [19], we extract the upper limit for the X parameter and thus get the following NMM limit:

$$\mu_\nu < 2.9 * 10^{-11} \mu_B. \tag{3.7}$$

The data is processed in the energy region of interest (ROI) from 2.8 keV to 55 keV with a step of 0.1 keV. The region from 9.4 keV to 11.2 keV is excluded as the corresponding peak could vary in time. The time dependence of the peak intensity is traced (Figure 9). As one can see after two months of data taking, it became almost constant. This peak has an internal origin, so it is always observed as complete absorption peak without low-energy compton

tail. Taking additionally into account that the intensity is rather small, we can state that the affection of this peak to the region below 9.4 keV due to finite energy resolution is negligible.

There are two kinds of possible systematic errors in the procedure of X-value extraction from experimental data. The first one arises from the uncertainties in knowledge of the neutrino energy spectrum and initial intensity as well as its distortions caused by possible short-baseline neutrino oscillations [22]. It includes also the uncertainty of the reactor thermal power, detector fiducial volume, and effective measurement time. Each of these terms enters the final result as *a factor* so that a sum of their relative errors gives a small rise only to the X-distribution width (~10%) but not the central value. That is why it is not very important for the case of upper limit estimation. The second source of systematic error originates from the background estimation. As it was mentioned, the idea of the experiment is to compare low-energy background measured for the reactor ON and OFF periods *ceteris paribus*. Nonequivalence of the conditions could either shift the mean value to the unphysical (negative) region or mimic the nonzero NMM value. It could be caused by the incorrect normalization of the measurement times $T_{\mathrm{ON}}/T_{\mathrm{OFF}}$ as well as by presence of any unrecorded background component correlated with the reactor operation. The absence of the above effects is demonstrated in Figure 8. One can see the deviation of central value X_0 from zero to be comparable with the dispersion σ. That proves the validity of our assumptions and the propriety of the chosen method for estimation of the upper limit on X-value.

4. Future Plans

At present time, we prepare experiment GEMMA-II. The experimental setup is being placed under the reactor number 3 where the distance from the centre of the core is 10 m. In this way, we double the antineutrino flux up to $5.4 \times 10^{13}\,1/\mathrm{cm}^2/\mathrm{s}$. The γ-background conditions in the new room are much better (by an order of magnitude), and the climate conditions are more stable. Furthermore, being equipped with a special lifting mechanism, the spectrometer will be moveable. It gives us an opportunity to vary on-line the antineutrino flux significantly and thus suppress the main systematic errors caused by the possible long-term instability and uncertainties of background knowledge. The mass of the detector is increased by a factor of 4 (two detectors with a mass of 3 kg each). To avoid the "Xe-problems," the internal part of the detector shielding will be gas tight. A special U-type low-background cryostat is used in order to improve the passive shielding and thus reduce the external background in the ROI down to ~0.5–1.0 $(\mathrm{keV{*}kg{*}day})^{-1}$. A special care is taken to improve antimicrophonic and electric shielding. We also plan to reduce the effective threshold from 2.8 to 1.5 keV. The neutrino flux monitoring will be available by means of special detector (project DANSS, to be published). As a result of all the improvements we will be able to suppress the systematic errors and expect the experimental sensitivity to be at the level of $1 \times 10^{-11}\,\mu_B$ and thus to reach the region of astrophysical interest.

5. Conclusion

The experimental NMM search with GEMMA spectrometer has been going on at KNNP (Russia) since 2005. The HPGe detector of 1.5 kg placed 13.9 m under the core of the 3 $\mathrm{GW_{th}}$ water moderated reactor has been exposed to the antineutrino flux of $2.7 \times 10^{13}\,1/\mathrm{cm}^2/\mathrm{s}$. As a result of the measurement (about 18000 ON-hours and 4500 OFF-hours of live time) the world best upper limit of $2.9 \times 10^{-11}\,\mu_B$ at 90% C.L. was set for the NMM.

The analysis of data indicates that the sensitivity limit of the setup is almost reached. To improve it we prepare significant upgrading of the spectrometer (GEMMA-II). Within the framework of this project we plan to use the antineutrino flux of $5.4 \times 10^{13}\,1/\mathrm{cm}^2/\mathrm{s}$, increase the mass of the germanium detector by a factor of four, and decrease the level of the background. These measures will provide us the possibility of achieving the NMM limit at the level of $1.0 \times 10^{-11}\,\mu_B$.

Acknowledgments

The authors are grateful to the Directorates of ITEP and JINR for constant support of this work and especially to M. V. Danilov for his important comments. The authors appreciate the administration of the KNPP and the staff of the KNPP Radiation Safety Department for permanent assistance in the experiment. This work is supported by the Russian State Corporation ROSATOM and by the Russian Foundation for Basic Research, Projects 09-02-00449 and 09-02-12363.

References

[1] M. B. Voloshin, M. I. Vysotsky, and L. B. Okun, "Neutrino electrodynamics and possible effects for solar neutrinos," *Journal of Experimental and Theoretical Physics*, vol. 64, pp. 446–452, 1986.

[2] M. Fukugita and T. Yanagida, "Particle-physics model for voloshin-vysotsky-okun solution to the solar-neutrino problem," *Physical Review Letters*, vol. 58, no. 18, pp. 1807–1809, 1987.

[3] S. Pakvasa and J. W. F. Valle, "Neutrino properties before and after KamLAND," *Proceedings of the Indian National Science Academy A*, vol. 70A, pp. 189–222, 2004.

[4] M. Gorchtein, N. F. Bell, M. J. Ramsey-Musolf, P. Vogel, and P. Wang, "Model independent naturalness bounds on magnetic moments of majorana neutrinos," in *Proceedings of the 14th International Conference on Supersymmetry and the Unification of Fundamental Interactions (SUSY '06)*, vol. 903 of *AIP Conference Proceedings*, pp. 287–290, June 2006.

[5] N. F. Bell, M. Gorchtein, M. J. Ramsey-Musolf, P. Vogel, and P. Wang, "Model independent bounds on magnetic moments of majorana neutrinos," *Physics Letters B*, vol. 642, no. 4, pp. 377–383, 2006.

[6] N. F. Bell, V. Cirigliano, M. J. Ramsey-Musolf, P. Vogel, and M. B. Wise, "How magnetic is the dirac neutrino?" *Physical Review Letters*, vol. 95, no. 15, Article ID 151802, 4 pages, 2005.

[7] N. F. Bell, V. Cirigliano, M. J. Ramsey-Musolf, P. Vogel, and M. B. Wise, "Magnetic moments of dirac neutrinos," in *Proceedings of the 17th Internatinal Conference on Particles and Nuclei*, vol. 842 of *AIP Conference Proceedings*, pp. 874–876, Santa Fe, NM, USA, October 2005.

[8] B. Kayser, "Neutrino properties," in *Proceedings of the Neutrino*, Christchurch, New Zealand, May 2008.

[9] C. Giunti and A. Studenikin, "Neutrino electromagnetic properties," *Physics of Atomic Nuclei*, vol. 72, no. 12, pp. 2089–2125, 2009.

[10] A. Studenikin, "Neutrino magnetic moment: a window to new physics," *Nuclear Physics B*, vol. 188, pp. 220–222, 2009.

[11] N. F. Bell, "How magnetic is the neutrino?" *International Journal of Modern Physics A*, vol. 22, no. 27, pp. 4891–4899, 2007.

[12] F. Reines, H. S. Gurr, and H. W. Sobel, "Detection of $\overline{\nu}_e - e$ scattering," *Physical Review Letters*, vol. 37, no. 6, pp. 315–318, 1976.

[13] P. Vogel and J. Engel, "Neutrino electromagnetic form factors," *Physical Review D*, vol. 39, no. 11, pp. 3378–3383, 1989.

[14] T. H. Wong et al., "Search of neutrino magnetic moments with a high-purity germanium detector at the Kuo-Sheng nuclear power station," *Physical Review D*, vol. 75, no. 1, Article ID 012001, 16 pages, 2007.

[15] A. G. Beda, V. B. Brudanin, E. V. Demidova et al., "First result for the neutrino magnetic moment from measurements with the GEMMA spectrometer," *Physics of Atomic Nuclei*, vol. 70, no. 11, pp. 1873–1884, 2007.

[16] D. W. Liu et al., "Limits on the neutrino magnetic moment using super-kamiokande solar neutrino data," *International Journal of Modern Physics A*, vol. 20, no. 14, pp. 3110–3112, 2005.

[17] C. Arpesella and The Borexino Collaboration, "Direct measurement of the ^{7}be solar neutrino flux with 192 days of borexino data," *Physical Review Letters*, vol. 101, no. 9, 6 pages, 2008.

[18] A. G. Beda, E. V. Demidova, A. S. Starostin, and M. B. Voloshin, "Low-background Ge-NaI spectrometer for measurement of the neutrino magnetic moment," *Physics of Atomic Nuclei*, vol. 61, no. 1, pp. 66–73, 1998.

[19] A. G. Beda, V. B. Brudanin, E. V. Demidova et al., "Status of the experiment on the measurement of the neutrino magnetic moment with the spectrometer GEMMA," *Physics of Atomic Nuclei*, vol. 67, pp. 1948–1952, 2004.

[20] E. Garcia, F. T. Avignone III, R. L. Brodzinski et al., "Dark matter searches with a germanium detector at the canfranc tunnel," *Nuclear Physics B*, vol. 28, no. 1, pp. 286–292, 1992.

[21] W.-M. Yao et al., "Review of Particle Physics," *Journal of Physics G*, vol. 33, no. 1, 2006.

[22] G. Mention, M. Fechner, T. H. Lasserre et al., "The reactor antineutrino anomaly," *Physical Review D*, vol. 83, no. 7, 20 pages, 2011.